Physics with REX-ISOLDE: from experiment to facility

Physics with REX-ISOLDE: from experiment to facility

P Van Duppen[1] and K Riisager[2]

[1] Instituut voor Kern- en Stralingsfysica, Department of Physics and Astronomy, K.U.Leuven, B-3001 Leuven, Belgium
[2] Department of Physics and Astronomy, Aarhus University, DK-8000 Aarhus C, Denmark

E-mail: piet.vanduppen@fys.kuleuven.be and kvr@phys.au.dk

Abstract
The REX-ISOLDE project and its physics program are presented. The innovative approach used to post-accelerate essentially all existing radioactive beams available at ISOLDE to 3 MeV u^{-1} is presented and beam properties are discussed. Isotopes as light as ^{8}Li and as heavy as ^{224}Ra have been used for Coulomb excitation, few-nucleon transfer reaction or fusion evaporation studies. Selected examples of the physics program, primarily utilizing the Miniball detector and segmented silicon detector arrays, are presented emphasizing some unique features of REX-ISOLDE. Finally, the HIE-ISOLDE project aiming at, amongst other goals, increasing the beam energy to 5.5 MeV u^{-1} and above, will be briefly discussed.

(Some figures in this article are in colour only in the electronic version)

1. Introduction and historical note

The rich physics outcome of nuclear-reaction studies employing unstable targets and projectiles was foreseen already from the mid-sixties [1], but although post-acceleration at ISOLDE was considered as early as 1977 (and encouraged by Specht in 1981) [2], earnest considerations were only given from the end of the eighties through the PRIMA proposal [3]. The main aim of PRIMA was to study the reactions of light nuclei of astrophysical relevance at energies up to about 1.4 MeV u^{-1}, similar to what was being implemented at the time in Louvain-la-Neuve [4]. The rapid progress in the field quickly made PRIMA obsolete and led to discussions in larger circles, at first with a UK community around the ISIS facility at Rutherford Appelton Laboratory [5].

Traditionally, experiments at the ISOLDE facility have taken place at low energy (up to 60 keV) via decay studies, ion (or atomic) beam measurements, ion manipulation e.g. in traps for mass measurements or implantation in host materials at temperatures from 10 mK upward

for detailed studies of the decay process or studies of host properties in solid-state physics and life science. An overview of the many possibilities can be found from the laboratory portrait [6] published a decade ago. The strength of the science program at ISOLDE has for many years been based on the combination of the large number of different isotopes that can be produced with many different techniques that can be employed to study them. It seemed natural to extend these techniques to include also reaction studies at moderate energies, such as Coulomb excitation, capture reactions and transfer reactions. The challenge was to devise an acceleration scheme that could take full advantage of the large range of isotopes available at ISOLDE.

The discussions in and around the ISOLDE community finally led to the REX-ISOLDE proposal in 1994 [7], the acronym coming from 'Radioactive beam EXperiments at ISOLDE'. Its key ingredient was an innovative charge breeding scheme combining bunching in a Penning trap with an electron beam ion source (EBIS), details will be given below. The philosophy was to separate as much as possible the production of singly charged radioactive ions from the subsequent ion manipulation to provide bunches of multiply charged ions needed for an efficient acceleration in all mass ranges. All components of REX-ISOLDE are therefore located inside the experimental hall which was helpful in the commissioning phase but places, at present, restrictions upon the intensity of some of the radioactive ion beams (RIB) to be accelerated. It was initiated as an experiment and the construction and initial running phase paid for by sources outside CERN. The transfer to and integration into the CERN accelerator departments only took place after the final commissioning. The first physics runs were performed late 2001.

Detailed descriptions of the design of REX-ISOLDE, its commissioning and technical performance so far have been given elsewhere [8–14]. We shall focus on the main physics results achieved up to now and on the prospects for future experiments. The unique capabilities of REX-ISOLDE build on and are enhanced by the variety of ion manipulation techniques developed for and employed by the low-energy experiments at ISOLDE. To give a better perspective of the possibilities inherent in the REX-ISOLDE scheme, we shall start by giving a brief overview of RIB production and acceleration at ISOLDE. Section 3 outlines the present experimental instrumentation that determines which experiments can be undertaken. Section 4 presents a selection of physics results obtained so far in more than 30 approved experiments. Finally, section 5 presents a brief outlook for the years ahead.

2. Radioactive beam production at ISOLDE

2.1. The ISOLDE facility

ISOLDE's RIB are produced using the 1.4 GeV proton beam from the PS-Booster accelerator at CERN. Beam pulses of about 3×10^{13} protons per pulse are send to the ISOLDE target every 1.2 s or multiples of this period resulting in an average beam intensity of 2 particle μA. Various solid and liquid target materials are used to produce a wide spectrum of radioactive isotopes covering essentially the whole nuclear chart below uranium ($Z = 92$). Radioactive isotopes are produced via proton-induced target fragmentation, spallation and fission reactions. The most frequently used target material is uranium carbide (UC_x). In 2007, it was used for 67% of the beam time, followed by SiC (9%) and liquid lead (6%). The radioactive products are thermalized in the target material and are subsequently transported from the target container to the ion source via diffusion and effusion processes. To speed up this process, the whole target–ion source unit is kept at high temperature, typically 2000 °C for e.g. a UC_x target. The speed of the diffusion and effusion process is governed by the physical and chemical properties of the
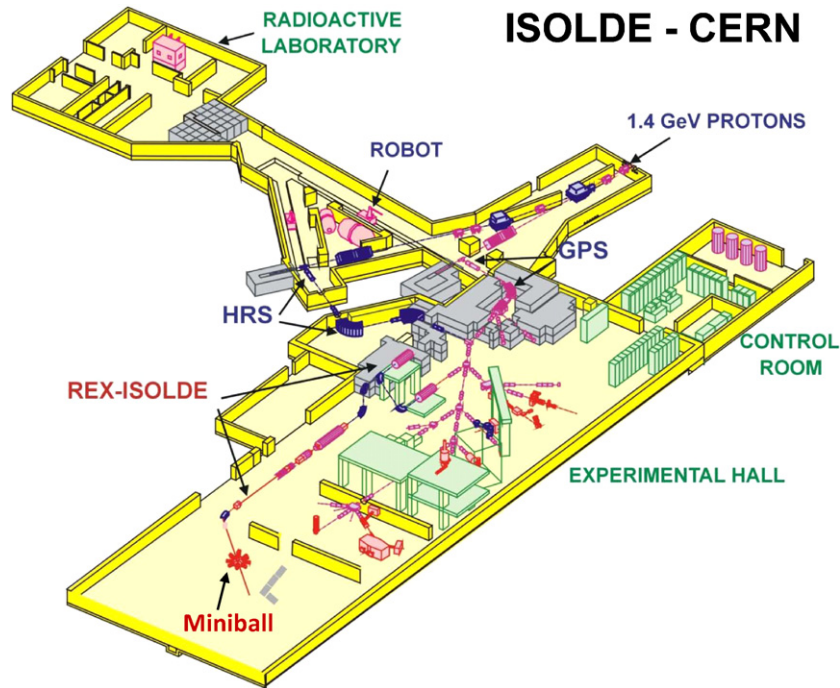
Figure 1. The layout of the ISOLDE facility is shown. The REX-ISOLDE accelerator complex can receive RIB from both mass separators (HRS: high resolution separator, GPS: general purpose separator). Two beam ports are currently available for experiments with the energetic beams.

radioactive elements of interest and of the specific materials that the target container, transfer line and ion source are made of. Consequently, radioactive isotopes that have small diffusion coefficients or very long lingering times at the surface of the target or container material, like the isotopes from some of the refractory elements, undergo radioactive decay before they are ionized and are thus lost. Once the atoms reach the ion source, a large fraction is ionized to a 1^+ charge state. Different ion sources are used at ISOLDE implementing different ionization mechanisms: electron impact ionization in high-temperature plasma sources and, surface and laser ionization in a hot cavity. The ions are subsequently extracted from the ion source, accelerated to typically 60 keV, mass separated according to the mass-over-charge ratio using a dipole magnet and sent to the different experimental set-ups. Recently, a radiofrequency cooler-buncher has been installed in the low-energy beam line allowing the delivery of short bunches of RIB to experiments without a substantial loss in intensity. This development has resulted in a substantial increase in the peak-to-background ratio for e.g. the collinear laser spectroscopy measurements [15]. For a general description of the ISOLDE facility, the reader is referred to [16]. A layout of the facility is shown in figure 1.

ISOLDE's decades of experience in target–ion source development to make the whole process, from isotope production in the target to beam delivery to the experimental set-up, efficient, fast and selective has resulted in a wide spectrum of beams. Radioactive beams with intensities reaching the nA level (e.g. ^{213}Fr with 8.4×10^9 particles s^{-1}) and of short-lived isotopes with a few milliseconds half-life (e.g. ^{14}Be, $T_{1/2} = 4.45$ ms) have been achieved. These beams are used for experiments in the field of nuclear physics and weak
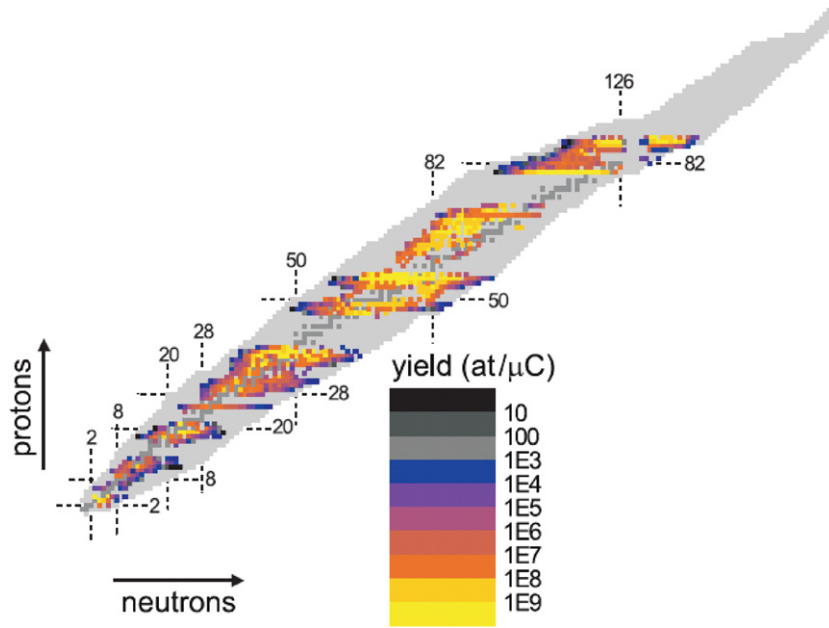
Figure 2. ISOLDE delivers beams that are used in an energy range from 10^{-6} eV (10 mK) to 3 MeV u^{-1}, with intensities up to 10^{10} ions s^{-1}, for isotopes with proton number from 2 to 88 and neutron number from 4 to 144; as light as ^{6}He to as heavy as ^{232}Ra. Over 800 RIB are available for experiments. The chart of nuclei is shown with a false color overlay of the radioactive beams available from ISOLDE. The color code gives the intensity of the 60 keV beams. The post-accelerated beam intensity can be obtained by multiplying the latter values with the total REX efficiency that can be obtained from figure 3 [22].

interaction studies (taking ~45% of the beam time), solid-state physics studies (~24%), atomic physics studies (~22%), particle and astrophysics studies (~10%) and biology and medicine (~4%). Figure 2 overlays on the nuclear chart the current beams and the intensity available at 60 keV. The gaps with no beams available correspond to refractory-type elements (e.g. the Ti ($Z = 22$)–V(23), Zr(40)–Rh(45) and Ta(73)–Pt(78) regions) or extremely short-lived isotopes (e.g. the $N = 128$–130 alpha emitting isotones with half-lives in the microsecond region). Next to the *intensity* is the *purity* of the final beam, an equally important parameter. Decades of RIB research has shown that different purification steps have to be applied sequentially as in most cases none of the purification steps result in a 100% pure beam. Different ways are implemented to purify ISOLDE's beams. The most straightforward way is to increase the wanted isotope over its isobaric contaminants by using the high-resolution mass separator [16]. Using the high-resolution mass separator, however, often induces losses in intensity. Other ways to purify the beam are making use of the physical and chemical properties of the element. For example, pure beams of gaseous elements are produced by cooling the transfer line between the target container and the ion source. In this way only the non-condensable elements (e.g. noble gases, gaseous molecules) are transferred to the ion source. Using surface ionization leads to beams of elements with low ionization potential (alkaline-like or earth alkaline-like elements). The most elegant and effective way to purify the ion beam is the use of the so-called resonant ionization laser ion source (RILIS) [17, 18]. Resonant laser ionization is an element selective process whereby atoms are irradiated by two or three lasers exciting the electron in

two or three resonant steps to the continuum. This allows the production of very pure beams as only atoms of the element of interest are ionized. Furthermore, because the nuclear spin determines the hyperfine structure of the atomic levels, isomeric beams can be produced. The RILIS is now used for more than half of the beam time and isomeric beams of isotopes from copper, silver, lead and polonium have been produced and used for experiments (see e.g. [19]). It should be noted that the pulse structure of the PS-Booster proton beam creates a particular time profile of the RIB depending on a combination of the release properties and the half-life of the isotope of interest [20]. The fact that this time profile can be very different for different isobaric isotopes is used to further purify the beam or to identify the experimental signals belonging to the isotopes under study (see e.g. [21]).

2.2. The REX-ISOLDE project

In order to boost the energy of the existing RIB of ISOLDE from typically 60 keV to a few MeV u^{-1}, a new concept was proposed whereby the existing singly charged ion beams from ISOLDE could be accelerated in a universal, fast, efficient and cost-effective way [7, 13, 14]. The concept is based on ion beam cooling and bunching in the buffer gas of a Penning trap [23], charge-state breeding in an EBIS [24] and post-acceleration in a room-temperature linear accelerator [25]. The original aim of the project was to prove the new concept's principle and to perform pilot experiments with short-lived post-accelerated RIB [7]. The 60 keV RIB from ISOLDE are retarded and continuously injected into a Penning trap situated at a high-voltage platform with a potential of nearly 60 kV. In the trap the ions are accumulated and at the same time cooled via buffer gas collisions. After a fixed time, which is determined by the required charge breeding time, the ion bunch is extracted from the Penning trap, accelerated to 60 keV, transferred to the EBIS and retarded to ground potential prior to injection into the EBIS. The typical duration of the ion bunches extracted from the Penning trap is 10 μs. After charge breeding to the required mass-to-charge ratio (A/Q) <4.5, the ion bunch is extracted from the EBIS, mass separated and injected into the radiofrequency quadrupole (RFQ) accelerator. The charge breeding time depends on the required charge-to-mass ratio and thus on the isotope of interest. It varies from typically 20 ms for light mass elements ($A < 40$) to over 200 ms for the heavy elements in the lead region ($A \simeq 200$). The typical time width of the ion bunch extracted from the EBIS is 100 μs. As the required injection energy for the RFQ is 5 keV u^{-1}, the EBIS platform potential is lowered from the 60 kV retarding potential down to ~20 kV while charge breeding takes place. The room-temperature accelerator typically runs with a 10% duty cycle (e.g. a radiofrequency-on period of 2 ms every 20 ms). The RFQ accelerator is followed by an interdigital H-type (IH) structure with a final energy between 1.1 and 1.2 MeV u^{-1}, three seven-gap resonators that create an energy range from 0.8 to 2.2 MeV u^{-1} and finally by a nine-gap resonator boosting the beam energy to a maximum of about 3 MeV u^{-1}. The time structure of the accelerated ions is shown in figure 2 of [14]. It is determined by the repetition rate of the proton beam pulse from the PS-Booster (a proton pulse every 1.2 s or an integer multiple of this period), the release profile of the isotope of interest from the ISOLDE target ion source unit (typically tens of ms to s scale), the duty cycle of the accelerator (typically one ~40 to 150 μs wide pulse from the EBIS every 20 ms) and the micro time structure of the linear accelerator (a few ns pulse width every 10 ns).

2.3. Specific RIB properties

The universal principle behind REX-ISOLDE allows the acceleration of literally all RIB available at ISOLDE currently up to an energy of 3 MeV u^{-1}. Beams as light as ^{8}Li and
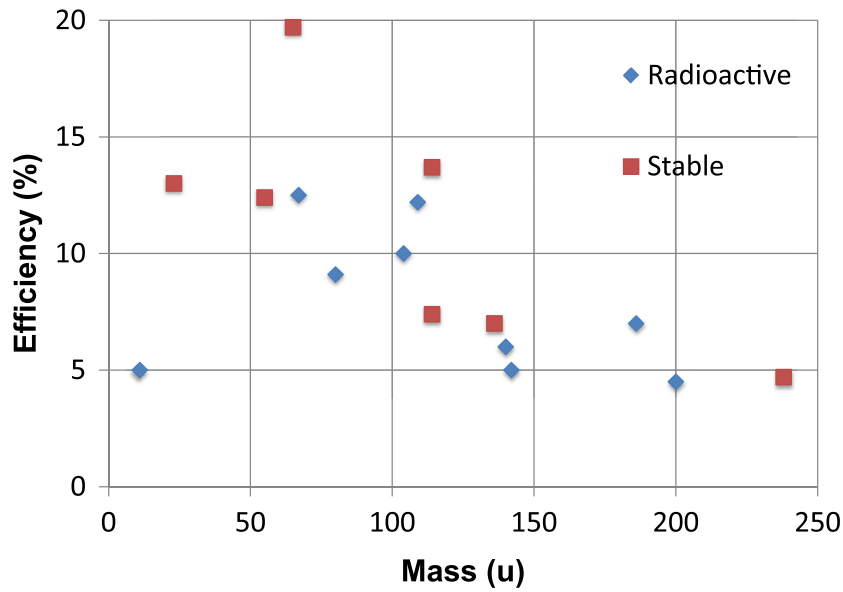
Figure 3. The product of the cooling, bunching and charge-state breeding efficiency is given as a function of mass. Values obtained for radioactive and stable isotopes are shown [13]. Tuning the REX bunching and charge-breeding system is easier with the higher intensity stable beams; therefore, on average the efficiency values for stable beams are higher than the values obtained on-line for radioactive isotopes. The acceleration efficiency at maximum energy reaches 85%. The original design values of the REX-ISOLDE project were an efficiency of 10% and $A < 50$ [7].

as heavy as ^{224}Ra have been accelerated with efficiencies varying from $\sim$2% to 10% (see figure 3). These efficiency data were obtained in off- and on-line conditions and illustrate the potential of the new RIB acceleration concept. The total time it takes to cool, bunch, charge breed and accelerate depends on the isotope of interest and is mainly determined by the charge breeding time necessary to obtain the A/Q ratio $<$4.5. It can be as fast as 12 ms in the case of ^{9}Li or up to about 400 ms for ^{204}Rn [13]. The purity of the accelerated beam depends on the production method of the isotope of interest, the target and ion source system used, the release time of the isotope of interest and of the contaminating isotopes and, again, the specific A/Q ratio used for the post-accelerated beam. Only by combining different selection principles based on physical, atomic and chemical properties can the required purity be reached. A number of experiments have profited from these developments and below we list some typical cases.

In the case of Coulomb excitation studies of ^{80}Zn ($T_{1/2} = 0.54$ s), the suppression of the isobaric contamination was crucial (see section 4.2.2) [26, 27]. When using the RILIS to produce a beam of ^{80}Zn, a strong isobaric contamination of ^{80}Rb and ^{80}Ga was observed. Rubidium and gallium have a low ionization potential and are swiftly surface ionized in the high-temperature cavity. In order to reduce the intensity of these contaminants, two strategies were adopted: the use of a proton-to-neutron converter and a quartz transfer line between the target and the ion source. The low-energy neutrons produced by the converter mainly induce fission on ^{238}U while spallation that produces ^{80}Rb is strongly suppressed [28] (see also figure 1 of [27]). Moreover, the use of a quartz transfer line between the target container and the hot cavity prevents many elements to reach the ion source as they condense on the walls

of the transfer line, except members of the chemical group 12 (zinc, cadmium, mercury). Thus, while the transfer of ^{80}Zn from the target to the RILIS is hardly delayed, a strong delay is induced for gallium resulting in a strong suppression of ^{80}Ga ($T_{1/2} = 1.7$ s) [29]. The next possible source of isobaric contamination in the accelerated beam stems from the EBIS. Beams from stable isotopes (such as carbon, oxygen, nitrogen, etc) are extracted from most ion sources. This can result in a strong isobaric contamination when the charge-to-mass ratio of the isotope of interest is similar to that of a stable isotope. However, because of its very clean vacuum conditions, an EBIS produces only relatively weak beams of stable isotopes and at several A/Q values virtually no stable beam is present. Finally, from the experimenters' point of view, the use of laser ionization allows one to perform proper background measurements and to identify weak signals by simply switching the lasers on- and off at regular time intervals (see figures 6 and 8 of [27]).

Another example of using the ion beam manipulation capabilities of the REX-ISOLDE system to produce new beams is the production of neutron-rich iron beams ($Z = 26$). Because of the chemical properties of iron, large delay losses are encountered in typical high-temperature thick target systems. However, RIB from the neighboring element manganese ($Z = 25$) are obtained with high intensity and purity thanks to the laser ionization. As it takes a certain time to manipulate the ion bunches in the Penning trap and in the EBIS system, and the fact that this time may be varied, the short-lived manganese isotopes can decay inside the Penning trap and/or EBIS system resulting in beams of neutron-rich iron isotopes. This technique was successfully tested with injected beams of the ^{61}Mn ($T_{1/2} = 0.71$ s) to produce beams of ^{61}Fe [30].

Since the time structure of the radioactive beam is dependent on the isotope of interest, analyzing the event time relative to the proton beam impact offers, in many cases, the possibility of further suppressing unwanted contamination. This technique was used in the Coulomb excitation experiment of ^{68}Ni to reduce the strong isobaric contamination of ^{68}Ga. The release of gallium isotopes is much faster compared to nickel; therefore, by setting proper beam gates or filtering the data in the off-line analysis the desired data can be obtained (see figure 1 of [21] and section 4.2.2).

A final example is the production of pure beams of ^{70}Se using a ZrO_2 fiber target; again this beam can be overwhelmed by isobaric contaminants (see section 4.3) [31]. The key producing a pure beam ^{70}Se for this measurement was to extract the beam as a 1^+ charged ^{70}Se^{12}C^{16}O molecule from the ISOLDE target–ion source system (in this case a high-temperature plasma ion source was used). This $A = 98$ beam, that is clean from any $A = 70$ contamination, is subsequently injected into the REX trap followed by the EBIS. In the latter, the molecules are dissociated under the electron bombardment and ^{70}Se is further charge bred until the required $Q = 19^+$ for post-acceleration is reached. This resulted in an isobarically pure post-accelerated ^{70}Se beam.

3. Instrumentation and experimental techniques

The experimental program at REX-ISOLDE focusses on Coulomb excitation, few-nucleon transfer reaction studies and fusion evaporation studies using radioactive beams. Dedicated instrumentation for γ-ray and charge particle detection was developed especially tailored to the particularities of RIB research: low beam intensities, low-γ-ray multiplicity and strong background radiation from the radioactivity of the beam itself.

For γ-ray detection, an array of six-fold segmented, individually encapsulated and tapered germanium crystals was constructed [32]. The so-called Miniball array is optimized with respect to full-energy peak efficiency and angular resolution rather than resolving power.

Miniball comprises eight cryostats, each containing three individual germanium crystals, which are mounted in close geometry around the target position. In its standard configuration for Coulomb excitation experiments, the typical target to detector distance is about 11 cm resulting in a solid-angle coverage of ∼60% of 4π. The photo-peak efficiency for 1.3 MeV reaches up to about 8%. The 24 detectors routinely used with the Miniball array result in a granularity of 144. By applying pulse shape analysis of the collected charges in each segment, 16 individual positions can be distinguished in each segment [32]. This results in an optimum granularity above 2000 for the present Miniball array. The granularity is essential to obtain proper Doppler corrected spectra as the RIB from ISOLDE have a typical velocity of 8.5% of the speed of light. However, with the present beam characteristics (typical diameter of 6 mm) and the close proximity of the germanium detectors, the inclusion of the position determination using pulse shape analysis does not substantially improve the Doppler correction over the use of the electronic segmentation. In the case of Coulomb excitation experiments, the spherical detection chamber is equipped with a double-sided silicon strip detector (DSSSD) of the CD type [33] to detect projectile and/or target particles. The DSSSD allows determining the energy (velocity) and scattering angle of the detected particles, an essential ingredient for the Doppler correction of the γ-ray spectrum. It covers an angular range typically from 16° to 53° in the forward direction (laboratory frame), although this range can be varied by changing the target to detector distance.

To study few-nucleon transfer reactions using RIB in inverse kinematics, two new detection set-ups were developed. The first, mainly used for scattering and transfer reactions with light nuclei [34–36], consisted of one or more 40 to 60 μm thick 16×16 double-sided Si strip detectors with a specially developed [37] thin dead layer, backed by 1000–1500 μm thick Si pad detectors. This set-up is typically adapted from run to run; one implementation is shown in figure 4 that also displays the second set-up, called T-REX (the T stands for transfer), mainly used for transfer reactions using heavier mass beams and combining particle detection with gamma detection [38, 39]. It consists of the Miniball array to detect γ-rays in coincidence with particles detected by an array of segmented Si detectors. The array of silicon detectors exhibits a nearly 4π angular coverage. The array comprises two CD detectors, in the forward and the backward direction, and a barrel of eight planar DSSSD's around 90°. The forward CD detector consists of two layers and is used as a △E-E telescope. The four forward detectors of the barrel are also △E-E telescopes. The △E detector (thickness 140 μm) is segmented in 16 strips perpendicular to the beam axis, and positional information along the stripes is obtained from the charge division on a resistive layer. The E detector is not segmented and has a thickness of 1000 μm. The four backward detectors are thick (500 μm), segmented E detectors. The use of △E-E telescopes in forward direction enables the identification of light particles (p, d, t, α).

4. Physics program

4.1. Light nuclei

The light nuclei is where we have the most intimate knowledge of the nuclear driplines [40] and it is therefore the natural starting point for investigations of nuclei as open quantum systems [41]. Among the phenomena seen here are nuclear halos [42], nuclear clusters and molecules [43] and changes in magic numbers [44]. Precision reaction experiments performed at a few MeV u^{-1}—such as elastic scattering, few nucleon transfer and fusion experiments—will give valuable information on the structure of light exotic nuclei, but one important aspect is that the dynamics of the reactions may change due to continuum effects. This adds to the richness
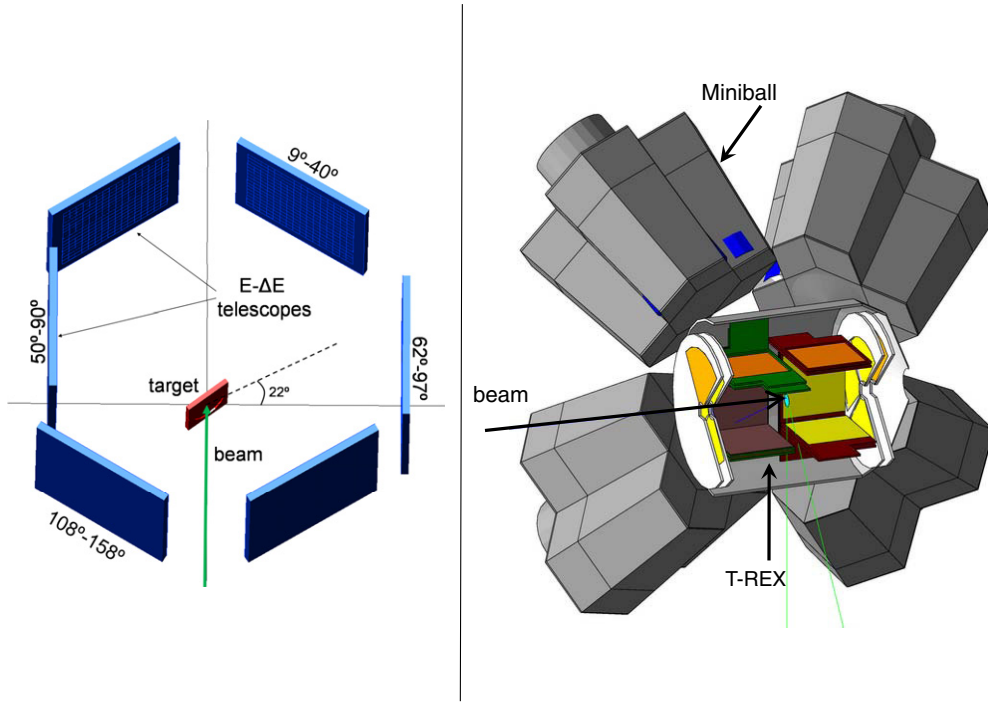
Figure 4. Left: the set-up used in the ^{11}Be scattering experiments [36, 61] mentioned in section 4.1. Right: the T-REX silicon barrel detector used in combination with the Miniball germanium array for few-nucleon transfer reaction experiments using the RIB from ISOLDE mentioned in sections 4.1, 4.2.1 and 4.2.2 (from [38, 39]).

of the physics in this region and in some respects still presents a challenge for the theoretical modeling.

Most of the interesting reaction channels will contain nuclei with quite low-level densities so that the resolution obtainable via the detection of the outgoing particles often suffices to uniquely identify the excited state of the populated nucleus. Gamma-ray detection is therefore not always needed and several experiments have taken place without the Miniball array in an optimized set-up.

A series of experiments with ^{9}Li were among the first initiated at REX-ISOLDE. The first runs [34, 45, 46] were performed at the original energy of 2.36 MeV u^{-1}, after the addition of the 9-gap resonator an energy of 2.77 MeV u^{-1} could be achieved. The nucleus ^{9}Li is the most neutron-rich $A = 9$ nucleus; it has a neutron separation energy of 4.064 MeV [47] and has one excited state at 2.69 MeV [48]. The main aim of the experiment was to acquire through the d(^{9}Li,p)^{10}Li reaction more detailed information on the structure of the unbound system ^{10}Li, required in order to obtain a coherent and complete description of the halo nucleus ^{11}Li. Several earlier experiments gave indications for the presence of both low-lying s- and p-wave states in the ^{9}Li+n system, see [40, 42] and references therein. The REX experiment confirmed this [46] through a simultaneous analysis of the energy spectrum and angular distribution within the coupled-channels born approximation (CCBA) formalism adapted for unbound final states. In this way all continuum–continuum couplings could be included. The p-state was found at 0.38 MeV, whereas the s-state appeared as a virtual state
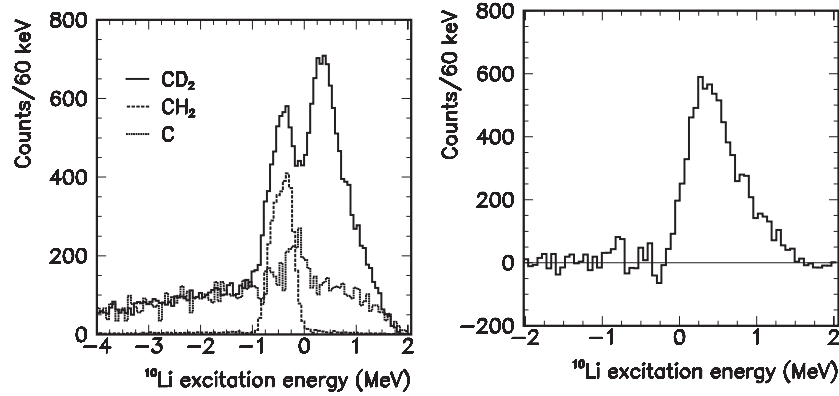
Figure 5. Count rate of the d(^{9}Li,p)^{10}Li reaction at 2.77 MeV u^{-1} [49] is shown as a function of the excitation energy of ^{10}Li. The left panel shows the spectrum recorded from a CD$_2$ target as well as (normalized) background spectra from CH$_2$ and pure C targets. The right panel gives the resulting final distribution.

with a negative scattering length 13–24 fm. Figure 5 shows the energy distribution of ^{10}Li with improved statistics from the most recent run [49] that still is under analysis. Since a CD$_2$ target with a few percent contaminant of CH$_2$ was used, separate runs on a pure C target and on a CH$_2$ target were made in order to control the background reactions.

The scattering in the d+^{9}Li system itself is actually also of interest since this is the final state in the beta-delayed deuteron decay of ^{11}Li where the decays apparently proceed directly into the continuum. The information from reaction experiments will therefore be crucial for constraining the interpretation of the decay experiment [50].

Among the other physics questions addressed by this experiment is the question of spectroscopic factors in light nuclei. The nuclei are so light that predictions can be made from *ab initio* calculations, but the ^{9}Li(d,t)^{8}Li data gave spectroscopic factors twice as large as predicted by theory [45] which could be due to the low reaction energy or to the fact that we are dealing with somewhat loosely bound systems. However, the same reaction done at ISAC at 1.68 MeV u^{-1} reported no problems [51] and seemed consistent with several ^{8}Li(d,p) results below 10 MeV u^{-1}, see e.g. [52]. This is an important point to settle since knock-out reactions at higher energy, e.g. at MSU [53], give a spectroscopic strength that varies systematically with the difference in separation energy between protons and neutrons. This must be checked [54] via low-energy transfer reactions that are a very well-understood probe closer to stability, one example being the systematic study of (d,p) and (p,d) reactions in ground-state to ground-state transitions [55], but it is important to note that the physical meaning of spectroscopic factors is still being discussed theoretically [56]. To see how transitions between the ^{8}Li and ^{9}Li nuclei behave will be an important check, but needs careful experiments that are analyzed in a consistent manner. First data have already been recorded at REX-ISOLDE with a ^{8}Li beam as shown in figure 6. The final theoretical analysis is being done presently, but it is already now clear that a standard distorted wave Born approximation (DWBA) is not sufficient to describe even the transition between the reasonably well bound ground states of ^{8}Li and ^{9}Li when one goes beyond the first maximum in the differential cross section. A significantly better job is done by employing the CCBA, i.e. it is crucial to get continuum effects under control before any physics conclusions can be drawn. Even the position of the first minimum is off in DWBA that only captures the very basic features of the reaction. This reinforces the need to cover an
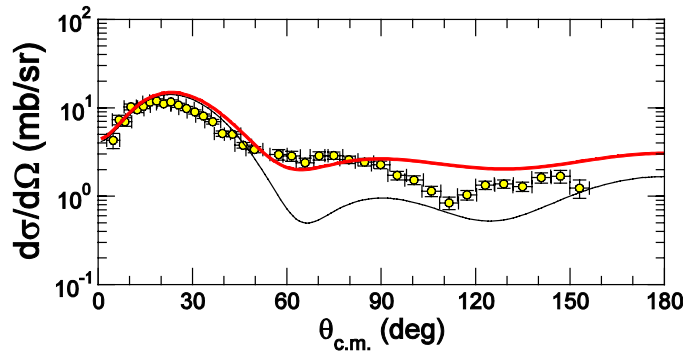
Figure 6. The differential cross-section for the d(^{8}Li,p)^{9}Li(gs) transition at 3.15 MeV u^{-1} is shown versus the angle in the center-of-mass system [35]. The lower curve is a DWBA calculation of the reaction and the upper curve a CCBA calculation, see the text.

extended angular range experimentally such that a more complete picture of the reaction can be obtained.

An intense beam of the halo nucleus ^{11}Be was developed at ISOLDE about a decade ago in order to enable precision measurements of its magnetic moment [57]. Several beta-decay experiments also benefitted from this development and it was logical also to undertake reaction measurements at low energy to complement and further elucidate the many results obtained earlier at higher beam energies for this prototype one-neutron halo. Transfer reactions can elucidate the structural changes between ^{11}Be and its neighbors ^{10,12}Be as shown by the p(^{11}Be,^{10}Be)d reaction performed at 35.3 MeV u^{-1} at GANIL [58] through which the amount of core excitation in the ^{11}Be ground state was probed or the recent ^{11}Be(d,p) reactions performed at 5 MeV u^{-1} at TRIUMF [59] where spectroscopic factors were extracted for states in ^{12}Be. A more extensive study of ^{12}Be through ^{11}Be+d reactions at 2–3 MeV u^{-1} has been initiated at REX-ISOLDE which very recently also included detection of gamma rays in the Miniball array.

The dynamics of reactions of halo nuclei with intermediate to heavy mass nuclei at energies close to the Coulomb barrier continues to present challenges [60]. Following initial experiments with the two-neutron halo nucleus ^{6}He, two experiments at REX-ISOLDE have contributed by investigating reactions on the one-neutron halo nucleus ^{11}Be (hoped to be simpler to treat theoretically) on ^{64}Zn [61] and ^{120}Sn [36]. In the former case, data were also recorded for ^{9}Be and ^{10}Be beams (at LNS-Catania and REX-ISOLDE, respectively) thereby allowing the better isolation of features unique to ^{11}Be. Whereas the Coulomb-nuclear interference peak, often referred to as the rainbow, is prominent in reactions with stable beams, the data show a clear suppression for ^{11}Be that furthermore sets in at smaller scattering angles. One way of understanding this feature is through enhanced coupling to low-lying continuum states. The enhanced role of break-up processes seen in earlier experiments at high energy therefore continues down to the Coulomb barrier.

4.2. Shell evolution

The nuclear shell model is very successful in describing the structure of atomic nuclei situated around closed proton and/or neutron shells. The availability of beams of exotic nuclei allows one to test particular aspects of the nuclear shell model very far from stability: evolution of

single-particle states, the disappearance and appearance of magic numbers and the validity of new effective interactions. Important progress in large-scale shell model calculations has been made in recent years [62, 63], new interactions have been proposed for the heavier fpg-shell region and especially the role of central and tensor forces has been highlighted [64, 65]. The region of the island of inversion around the $N = 20$ closed neutron shell, the neutron-rich nickel region ($Z = 28$) and the neutron-deficient and neutron-rich tin region ($Z = 50$) has been investigated at ISOLDE using Coulomb excitation and few-nucleon transfer reactions.

4.2.1. The N = 20 region. The island of inversion around ^{32}Mg($N = 20$) has been intensively studied using complementary methods which resulted in a wealth of data. Beta-decay studies, laser spectroscopy measurements and mass measurements all indicated unusual properties for the ground-state and low-lying excited states of the neutron-deficient isotopes around ^{32}Mg (see e.g. [44, 66]). The availability of energetic RIB of ^{32}Mg and nuclei in its neighborhood allowed the study of this phenomena in more detail and further in-beam spectroscopy (see e.g. [67]), Coulomb excitation (see e.g. [68]) and transfer reaction studies (see e.g. [69]) were performed. The combination of these experimental data and new theoretical calculations (see e.g. [70, 71]) delineated the so-called island of inversion and proposed as a driving mechanism to explain these observations multiparticle—multihole (p–h) excitations across the $N = 20$ shell. This hypothesis gives rise to specific properties that can be probed using different experimental techniques: (i) particle–hole excitations through a closed shell configuration result in an increased collectivity as it enhances the number of active nucleons and thus the number of deformation driving proton–neutron interactions; (ii) spin and parities, and the single-particle nature of some low-lying states should reflect excitation across the $N = 20$ shell and (iii) a 0$^+$ state presumably of a neutron two-particle–two-hole (2p–2h) nature should co-exist with the ground-state configurations or could even become the ground state. A sensitive probe to study collective properties is Coulomb excitation by which we may deduce transition or diagonal matrix elements between or of excited states. Single-particle properties of the low-lying states can be probed using one-neutron transfer reactions while the existence of excited 0$^+$ states and the study of their 2p–2h character can be probed using two-neutron transfer reactions of the type (t,p). At REX-ISOLDE Coulomb excitation, experiments using low-energy beams of ^{30,32}Mg were performed [72, 75]. The γ-ray spectra from which the $B(E2 : 0^+–2^+)$ results of ^{32}Mg ($T_{1/2} = 95$ ms) were extracted are shown in figure 7. The final result is currently being prepared for publication [73]. By comparing the intensity in the γ rays observed in the top and bottom spectrum the $B(E2 : 0^+–2^+)$ for ^{32}Mg can be extracted based on the known transition matrix elements of the γ-ray observed in ^{107}Ag. In this manner, the result does not depend on the absolute radioactive beam intensity, the target thickness or the absolute γ- and particle detection efficiency. Only the relative γ-ray efficiency and the purity of the RIB must be determined. The results firmly establish an increase in collectivity in ^{32}Mg when moving from ^{30}Mg, that exhibits a low degree of collectivity, to the $N = 20$ neutron shell closure. Essential for this and other measurements at REX-ISOLDE was not only sufficient beam intensity but, sometimes more importantly, the high degree of beam purity and the possibility of measuring the beam purity accurately using proper detectors or simply using the possibility of switching the lasers on and off during the experiment. Apart from intensive Coulomb excitation measurements, one-neutron and two-neutron transfer reactions have been performed on ^{30}Mg. From the first d(^{30}Mg, p)^{31}Mg experiment using a set-up with only a limited angular coverage for the proton detection, no definite conclusions could be drawn [74]. With the new T-REX set-up, d(^{30}Mg, p)^{31}Mg was repeated and the two-neutron transfer on ^{30}Mg was studied using a radioactive tritium target (t(^{30}Mg, p)^{32}Mg) [39, 76]. The tritium target was a thin strip of 500 μg cm^{-2} thick metallic Ti foil loaded with an atomic ratio ^{3}H/Ti
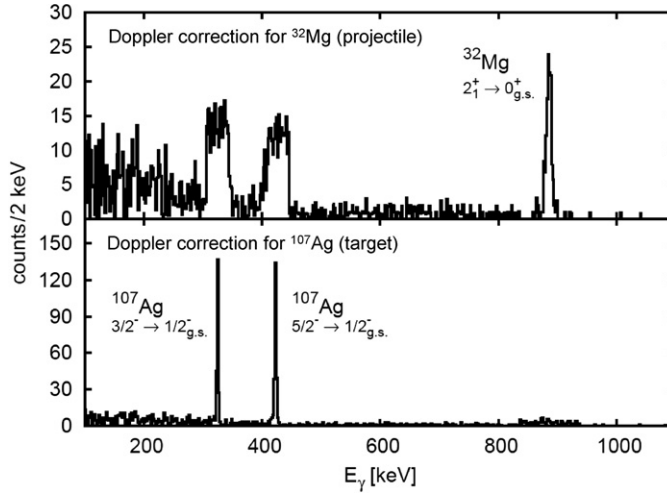
Figure 7. γ-ray spectra obtained after Coulomb excitation of a ^{32}Mg beam at 2.84 MeV u^{-1} on a 4.4 mg cm^{-2} thick ^{107}Ag target are shown after proper Doppler correction for the projectile (top) and for the target nuclei (bottom). The known transitions in ^{107}Ag and the 2$^+$–0$^+$ in ^{32}Mg are clearly identified. Note the very low background conditions (adapted from [75]).

of 1.5 corresponding to a target thickness of 40 μg cm^{-2} of tritium. Typical beam intensities of a few times 10^4 particles s^{-1} were used. The two-neutron transfer experiment clearly revealed the existence of an excited 0$^+$ state in ^{32}Mg at an excitation energy of 1058 keV. Figure 8 shows the proton angular distribution obtained for the ground state and the newly identified excited state. From the angular distribution, it can be concluded that this state is a 0$^+$ state only 178 keV above the known 2$^+$ state in ^{32}Mg. From the experimental cross section of the ground state population, it could be concluded that the ν2p3/2 contribution as deduced from Monte Carlo shell-model calculations is underestimated, while the cross section to populate the excited 0$^+$ state can be fairly well described within a shell-model interpretation assuming rather pure sd configurations [76].

4.2.2. Neutron-rich region around Z = 28. The experimentally observed nickel ($Z = 28$) isotopes span a very wide range including a number of doubly closed shell nuclei from ^{48}Ni, where two-proton ground state decay was observed [77], over ^{56}Ni, where enhanced core polarization has been observed [78, 79] toward ^{78}Ni, a nucleus of particular interest for nuclear structure and nuclear astrophysics [80]. This region of the nuclear chart thus represents an ideal testing ground for large-scale shell model calculations and the new interactions used. In addition ^{68}Ni, with its $N = 40$ sub-shell closure, is an interesting case as the importance of this shell closure, a parity changing harmonic oscillator closure, is still debated. The first excited state of ^{68}Ni is a 0$^+$ state and the first 2$^+$ state is located at a high excitation energy while the $B(E2 : 0^+–2^+)$ value appears to be low compared to the neighboring nuclei. Although this might be interpreted as a signature for a strong shell closure, it has recently been suggested that the parity change between the $\nu p_{1/2}$ and $\nu g_{9/2}$ neutron orbitals and the small angular momentum of the former are the cause of the observed phenomena [44]. The structure of the neighboring nuclei of ^{68}Ni (coupling one proton or one neutron particle or hole) studied in beta decay can be reasonably well described as core-coupled states but indicate at the same time the importance of neutron excitations through $N = 40$ and proton excitations through $Z = 28$
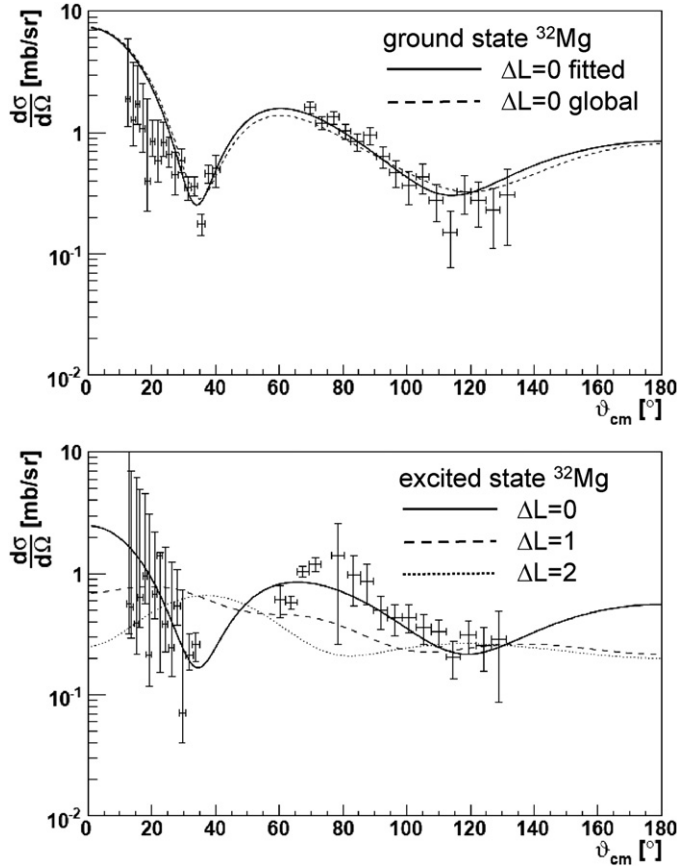
Figure 8. Proton angular distributions for the population of the ground state (top) and excited state at 1058 keV (bottom) in the ^{30}Mg(t, p)^{32}Mg reaction. The curves in the top panel are from DWBA calculations using fitted (solid) and global (dashed) optical model parameters. The curves in the bottom panel include DWBA calculations for $\Delta L = 0$, 1 and 2 transfer. The excited state is populated with $\Delta L = 0$ transfer leading to the identification of a 0_2^+ in ^{32}Mg (adapted from [76]).

(see e.g. [81]). The importance of proton excitations through the $Z = 28$ closed shell is e.g. well demonstrated by the recent observation of a low-lying long-lived $(1/2^-)$ isomer in ^{67}Co ([82], recently confirmed in [83]); taking away only one proton from ^{68}Ni already induces the obliteration of the $N = 40$ sub-shell gap and sets in a region of deformation below $Z = 28$.

In order to obtain a better understanding of the evolution of the nuclear structure between $N = 40$ and $N = 50$, Coulomb excitation experiments were performed using post-accelerated beams of ^{68}Ni [21], of the ground state and the long-lived isomers in ^{68,70}Cu [84], of the neutron-rich odd-mass copper isotopes ($^{67-73}$Cu) [85], of the neutron-rich zinc isotopes up to ^{80}Zn at the closed $N = 50$ neutron shell [26, 27] and of the neutron-rich manganese and iron beams [30]. The ^{68}Ni experiment confirmed the low value for the $B(E2 : 0^+ – 2^+)$ that was previously deduced from intermediate-energy Coulomb excitation [86], and the study of the ^{68,70}Cu isomers confirmed the core-coupled character of the states probed in the experiments and indicated only weak polarization effects induced by the extra-proton and neutron coupled to the ^{68}Ni. However, including data from ^{72}Cu shows that the coupling of at least two like
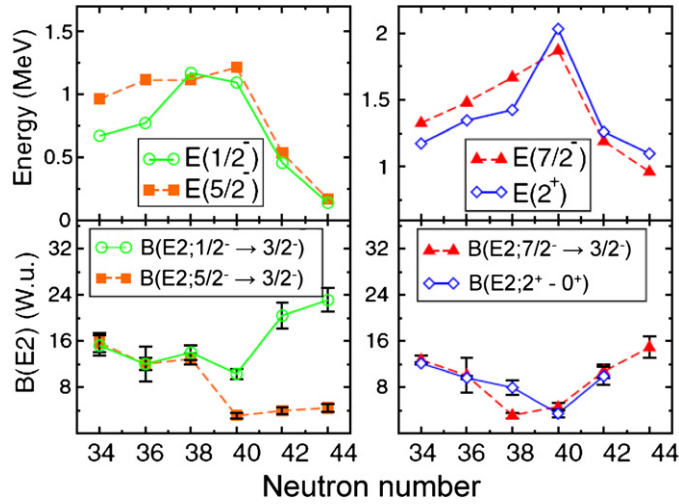
Figure 9. Top: the energies of the $1/2^-$, $5/2^-$ and core-coupled $7/2^-$ states in odd mass $^{63-73}$Cu along with the 2^+ levels in the corresponding even–even $^{62-72}$Ni are shown. Bottom: experimental $B(E2)$ values in $^{63-73}$Cu and $^{62-72}$Ni. Note the similarity between the energies and $B(E2)$-values of the $7/2^-$ and 2^+ states (right), the abrupt change in the structure of the lowest lying $5/2^-$ state and the increase in the collectivity of the $1/2^-$ state at $N = 40$ (adapted from [85]).

quasi-particles to ^{68}Ni weakens the stabilization effects of the $N = 40$ sub-shell and $Z = 28$ shell gaps [84]. These phenomena were further explored in the Coulomb excitation study of the odd-mass copper isotopes and revealed, at low excitation energy, a clear interplay between single-particle and collective effects in the odd-A copper isotopes beyond $N = 40$. These isotopes were, prior to the Coulomb excitation experiments, characterized by a $3/2^-$ ground state and a low-lying $5/2^-$ state whose excitation energy decreased dramatically beyond $N = 40$ when moving toward $N = 50$ [87]. The low $B(E2)$ value between these two states confirmed their single-particle nature. But surprisingly, strong excitation was observed toward a low-lying $1/2^-$ state, that followed the excitation energy behavior of the $5/2^-$ state very closely, indicating a strong enhancement of collectivity in these neutron-rich copper isotopes as shown in figure 9 [85]. The experiment also allowed the identification of the $(7/2^-)$ core-coupled state as its energy and $B(E2)$ values are very similar to those of the 2^+ state in the neighboring even–even nickel isotopes. In these series of neutron-rich copper isotopes, two $(7/2^-)$ states were identified from previous studies. The fact that only one of them is populated in Coulomb excitation points to a single-particle character for the other one; suggesting it to be a plausible candidate for a proton intruder state based on a $\pi(1p–2h)$ excitation across $Z = 28$.

Recent large-scale shell-model calculations performed with a new interaction for the fpg-shell nuclei in a valence space defined around the ^{56}Ni core were able to reproduce the trend of the $5/2^-$ state excitation energy; however, they failed to reproduce the properties of the $1/2^-$ state (see figure 13 from [62]). Another recent calculation performed in a valence space outside the ^{48}Ca core and including adjustments to reproduce the experimental $B(E2)$ value recently obtained in ^{80}Zn (see further) obtains a better agreement indicating the importance of proton excitations across $Z = 28$ to explain the collective structures observed in the neutron-rich copper isotopes [88]. Explaining the presence of spherical single-particle states, core-coupled states and collective states in the low-energy part of the isotopes at and around $Z = 28$ remains
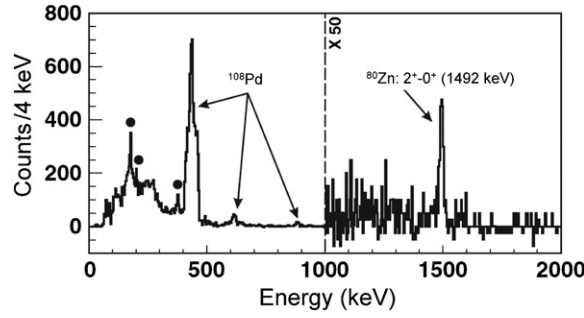
Figure 10. The Doppler corrected γ-ray spectrum for beam particle detection obtained after Coulomb excitation of a 2.79 MeV u^{-1} ^{80}Zn beam with an intensity of $\sim$3000 particles s^{-1} on a 2 mg cm^{-2} thick ^{108}Pd target is shown. The 2$^+$–0$^+$ transition in ^{80}Zn and known transitions in ^{108}Pd are indicated together with transitions from beam contaminant ^{80}Rb (circles) (adapted from [26]).

a challenge for theory and will have an impact on our understanding of the structure of the doubly magic ^{78}Ni. For completeness, we note that very recently the ground state spin and parity of ^{75}Cu have been determined by collinear laser spectroscopy to be $5/2^-$ confirming the anticipated crossing of the $5/2^-$ and $3/2^-$ states [89]. The latter measurements made it possible to propose a level scheme for ^{75}Cu [88].

The Coulomb experiments using the neutron-rich ^{74,76,78,80}Zn beams allowed to determine the first excited 2^+ state energy and the $B(E2 : 0^+–2^+)$ in the semi-magic ^{80}Zn($N = 50$) nucleus only two neutrons away from ^{78}Ni. The γ-ray spectrum obtained after Coulomb excitation of a ^{80}Zn beam with an intensity of $\sim$3000 particles s^{-1} accumulated for $\sim$100 h is shown in figure 10. The spectrum shows what can be achieved with Coulomb excitation experiments using weak RIB. Figure 14 of [27] shows the schematics of the 2^+ energy and the $B(E2 : 0^+–2^+)$ value for the $N = 50$ isotones compared to predictions from shell-model calculations using ^{56}Ni as a core. The shell-model calculations assume only protons as active valence particles, and a good agreement with the data is obtained provided large effective charges are used. This indicates a good $N = 50$ shell closure and an important $Z = 28$ core polarization around ^{78}Ni. However, none of the present shell-model calculations using ^{56}Ni as a core reproduce the energy of the first excited 2^+ state in the neutron-rich zinc isotopes beyond $N = 40$ properly, while the $B(E2)$ values are in reasonable agreement with experiment for the most exotic ones (see e.g. figure 8 from [62] and figure 13 from [27]). This problem remains to be solved.

Recently, one-neutron transfer reaction studies were also performed using a beam of ^{66}Ni at 3 MeV u^{-1}. A multitude of states up to 6 MeV excitation energy were populated in the d(^{66}Ni, p)^{67}Ni reaction, some of them exhibiting a strong ground-state gamma transition. The results, currently under analysis, will reveal spins and parities, cross sections and decay patterns of the populated levels. The high intensity of the ^{66}Ni beam (a few times 10^6 particles s^{-1}) and the high purity (>95%) will enable the study of the t(^{66}Ni, p)^{68}Ni reactions, probing explicitly neutron pairing properties in ^{68}Ni.

4.2.3. The tin region: toward ^{100}Sn *and around* ^{132}Sn. The tin nuclei, with the closed $Z = 50$ proton shell, are notorious examples of nuclei that can be described using the general seniority scheme. For example, the excitation energy of the first excited 2^+ is nearly constant throughout the whole isotopic chain from $N = 52$ to 80. In this scheme, the $B(E2 : 0^+–2^+)$

value is expected to show a parabolic behavior with a maximum value mid-shell between $N = 50$ and 82 and zero in ^{100}Sn and ^{132}Sn. The parabolic trend of the $B(E2 : 0^+–2^+)$ is also predicted by large-scale shell-model calculations and was indeed well confirmed by an extended set of data on the neutron-rich tin isotopes [90]. Recent results from intermediate energy Coulomb excitation experiments, however, seem to deviate from this trend. In order to confirm and to extend these findings to nuclei closer to ^{100}Sn, beams of ^{106,108,110}Sn were used to perform Coulomb excitation measurements at the so-called safe energies [91, 92]. The results clearly show a deviation from the parabolic trend of the $B(E2 : 0^+–2^+)$ and an increase in transition strength when going to lighter nuclei approaching ^{100}Sn. Using different nucleon–nucleon interactions in a large-scale shell-model approach could not reproduce these findings. Along the same lines, experiments were performed using ^{100,102,104}Cd ($Z = 48$) [93]. These experimental findings clearly request further theoretical investigations of the structure around ^{100}Sn.

Neutron-rich nuclei around ^{132}Sn have also been studied using Coulomb excitation in order to investigate the influence of the $N = 82$ and $Z = 50$ shell closures. Data were obtained with beams from even mass $^{122–126}$Cd, $^{138–144}$Xe and ^{140,142}Be isotopes [94]. These experiments were partially triggered by a surprising result obtained at the Oak Ridge radioactive beam facility [95, 96]. Experiments using neutron-rich tin and tellurium beams in the vicinity of ^{132}Sn showed a deviation from the simple picture that the product of the energy of the first 2^+ state with $B(E2)$ value can be described by a simple formula, the so-called Grodzins' formula [97]. The data are currently under analysis, but the new data combined with recent life-time measurements should resolve this issue.

4.3. Shapes and shape coexistence

Coulomb excitation is an ideal probe to investigate shapes and shape coexistence phenomena (see e.g. [98]). Beams from REX-ISOLDE have been used in different regions of the nuclear chart along $N = 20$ (see section 4.2.1), along the $N = Z$ line, along the krypton and strontium isotopic chain where abrupt changes in the ground state deformation are observed and in the neutron-deficient region around $Z = 82$. These data can be used to test beyond mean-field calculations or symmetry-based models, and eventual deficiencies between data and calculation might highlight missing ingredients in the model (see e.g. [99, 100] and references therein). Here we limit ourselves to a short discussion on the ^{70}Se and the light mercury isotopes.

The Coulomb excitation cross section using a ^{70}Se beam on a ^{104}Pd was deduced and used to calculate the $B(E2 : 0^+–2_1^+)$. However, the final result on the latter depends on the diagonal matrix element $\langle 2_1^+ \| E2 \| 2_1^+ \rangle$. By including the lifetime of the 2_1^+ state in the Coulomb excitation analysis, constraints on the sign and magnitude of $\langle 2_1^+ \| E2 \| 2_1^+ \rangle$ were put. Based on these findings, it was concluded that the ground state was, most likely, prolate [31]. However, a new measurement of the lifetime of the 2_1^+ [101] was in strong disagreement with the literature value and the conclusion drawn by [31] had to be revised. The 2_1^+ of ^{70}Se, and most probably also its ground state, are of oblate nature in agreement with Hartree–Fock–Bogolyubov-based configuration-mixing calculations [101].

The neutron-deficient mercury isotopes and nuclei in the neighborhood of the $Z = 82$ closed proton shell with neutron number around $N = 104$, midshell between $N = 82$ and 126, are prototype examples of shape coexistence. One of the earliest experimental indications for shape coexistence came from the mean-square-charge-radii measurements using optical spectroscopy techniques, showing a strong shape staggering between the even-mass and odd-mass mercury isotopes with $A < 186$ [102]. Meanwhile, a wealth of data on
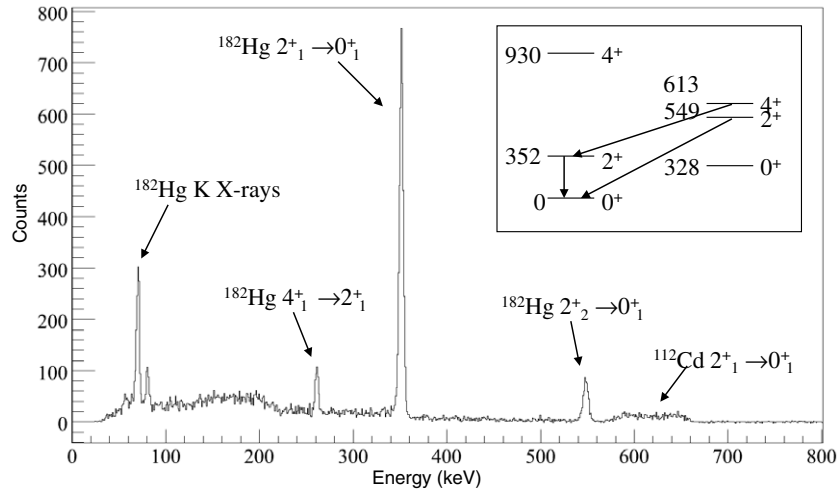
Figure 11. Part of the particle-gated gamma spectrum obtained after Coulomb excitation of ^{182}Hg on a ^{112}Cd target that was Doppler corrected for transitions in ^{182}Hg. The inset shows the partial level scheme of ^{182}Hg where the observed transitions are indicated with an arrow. The broad bump around 620 keV is the 2^+–0^+ transition in ^{112}Cd due to target excitation. The population of non-yrast states and an excess of Hg x-rays are observed. The former will be strongly enhanced with HIE-ISOLDE energies (see section 5).

mean-square-charge-radii in other isotopic chains, on coexisting rotational bands in several of these nuclei, on lifetimes of excited states, on fine-structure alpha-decay data and on low-lying excited 0^+ states has been collected, with the discovery of triple shape-coexistence in the $N = 104$ nucleus ^{186}Pb as probably the most intriguing aspect [103]. Little is known, however, on the matrix elements connecting the different states of the excited bands, nor on the sign of the deformation of the different bands. In order to shed light on these particular questions, Coulomb excitation experiments on the neutron-deficient mercury, lead, polonium and radon isotopes have recently been initiated. For these experiments, mass ($\sim$200) beams were accelerated, a mass region that was far from being included in the initial REX-ISOLDE project. High-quality datasets were obtained as can be seen in, e.g., figure 11 that shows the particle-gated gamma-ray spectrum obtained for ^{182}Hg [104]. The data are currently under analysis. The excitation of the 2_1^+, 2_2^+ and 4_1^+ is clearly observed. These first experiments clearly show the possibility of populating and studying non-yrast states whose properties are very important to understand shape coexistence. It is interesting to note as well that a large amount of mercury X-rays were observed, indicating that the 0_2^+ state or that levels, decaying via strongly converted transitions, were populated. The latter is important as E0 transitions are considered to be fingerprints for shape coexistence. To pin down the final analysis and interpretation of these findings, the Coulomb excitation experiments are complemented with life-time and conversion-coefficient measurements [105].

4.4. Other techniques

In addition to the above-mentioned program of Coulomb excitation and few-nucleon transfer reactions, other techniques have been and will be used at the REX-ISOLDE facility. The use of the transient field method in inverse kinematics to determine the sign and magnitude of the magnetic moment of the first excited 2^+ state in ^{72,74}Zn is planned. These experiments can
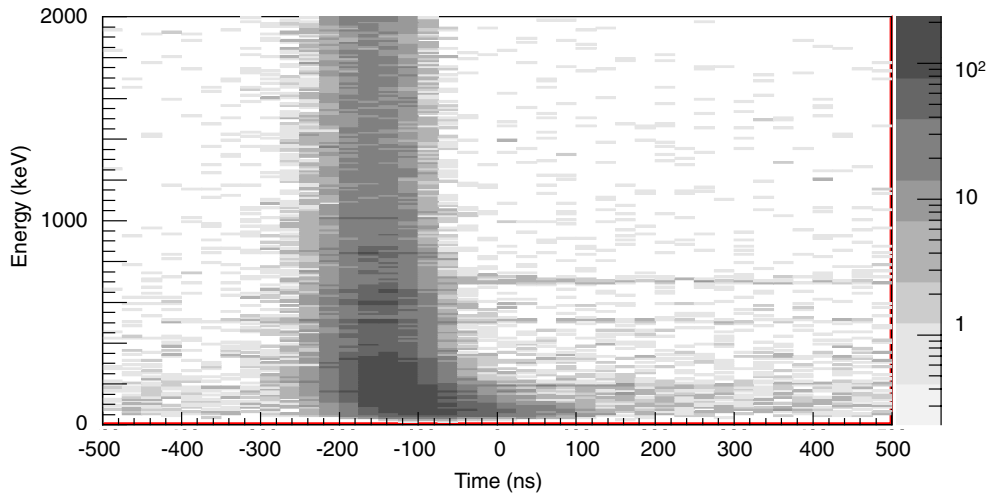
Figure 12. The energy recorded in Miniball for coincidences between a Miniball detector and a charged particle detector is shown versus the time difference between the two detectors. Prompt coincidences are situated around -150 ns. The line extending to the right at 690 keV is due to neutrons from $d(^{11}Be,n)$ events that are detected in Miniball via $^{72}Ge(n,n')$ to the 444 ns 0^+ level. See the text.

provide important insights into the wavefunction of these excited states, for example, regarding the importance of the neutron $g_{9/2}$ component in the zinc case [106]. Another technique that is currently under study is the so-called tilted foil technique to produce polarized beams [107]. The possible energy domains of the REX accelerator and its energy variability are ideally suited for this in-flight technique that, combined with a beta-NMR set-up, is especially interesting to study ground state magnetic or quadrupole moments of isotopes that are not readily amendable to laser techniques or have a very short half-life. The optimum energy needed may vary from case to case, but varies from 0.1 up to about 1–2 MeV u^{-1}, indeed an ideal window for the REX accelerator. The tilted-foil technique coupled to a beta-NMR set-up is also of interest for condensed matter research. The implantation of polarized radioactive probes in solid-state matrices gives direct information on the electronic and lattice structure of the sample under study. In combination with the large variety of RIB available, this potentially makes a very interesting research direction. Along the same lines, plans are under way to use the higher beam energy to obtain deeper implantation profiles to perform e.g. diffusion studies with conventional radioactive tracer techniques.

Finally, it is interesting to mention that modern Ge detector arrays are also reasonably efficient for neutron detection as demonstrated recently in a stable beam experiment [108]. The inelastic scattering of neutrons to the 0^+ excited state in ^{72}Ge that decays by emitting a 690 keV conversion electron gives a particularly clear signal that will be recorded at the ^{72}Ge position in the crystal, i.e. the direction of the original neutron can be extracted (in contrast, its energy will not be recorded). It is remarkable that the detection conditions are sufficiently clean at REX-ISOLDE that this neutron signature can be identified even with a radioactive ^{11}Be beam at 2.85 MeV u^{-1} of intensity about 10^5 ions s^{-1}. As shown in figure 12 the neutron signature is visible already in the raw dataset as slightly delayed coincidences between Miniball and the charged particle detector array.

4.5. Astrophysics

Experiments that are mainly motivated by astrophysics questions are a small component of the physics program at REX-ISOLDE compared to other facilities presented in this volume [4, 95, 109]. Some of the advancements of our knowledge on nuclear structure mentioned above will of course also improve the reliability of nuclear astrophysics calculations, see also [110]. Among the many facets of nuclear astrophysics [111], radioactive beams are mainly useful for explosive events [112] such as novae [113] or x-ray bursts.

The conditions for breakout of the hot CNO cycle are still investigated for the latter two events, one of the key processes being the reaction $^{14}O(\alpha,p)^{17}F$ that proceeds mainly through a resonance in ^{18}Ne at 6.15 MeV excitation energy. A recent experiment at REX-ISOLDE [114] studied the inelastic proton scattering of a post-accelerated ^{17}F beam in order to determine more precisely the decay properties of the 6.15 MeV state.

The inelastic proton branch, identified through coincidences between a proton group at 2.26 MeV and 495 keV γ-rays detected in the Miniball array, was consistent with a strong inelastic proton branch approximately equal in intensity to the ground-state branch. Combining this result with other experiments [95], it appears that ^{14}O will be destroyed through the (α,p) reaction in X-ray bursts, but not in novae, and that the inelastic branch will indeed make a significant contribution.

A typical feature of this experiment is that information on the astrophysically interesting reaction is obtained indirectly since the direct reaction rates are small, although not as prohibitively small as for non-explosive burning. The limits on the available beam time at ISOLDE indicates that the main contribution of REX-ISOLDE in this field in the future will be for reactions with beams that are unique for ISOLDE or for reactions where superior selectivity is offered by the ISOLDE-REX-Miniball combination.

5. Outlook and conclusion

Although REX-ISOLDE soon can celebrate its tenth anniversary, we are really only at the beginning of the exploitation of the possibilities emerging by having post-accelerated beams at ISOLDE. By late 2009, REX-ISOLDE had accelerated 72 different radioactive isotopes (of 25 elements), which is no more than about 10% of the radioactive isotopes that ISOLDE can deliver.

There are several regions of the nuclear chart that are not yet explored like e.g. the rare earth region or the heavy mass region around and above ^{208}Pb. Among the subjects that new experiments currently are starting to look into are octupole collectivity with recent Coulomb experiments using beams as heavy as ^{224}Ra and mixed symmetry states, but many more remain.

An important lesson to remember for the future is that new techniques developed for measurements at low energy, typically those involving ion manipulation with traps, coolers and lasers but also other 'tricks' that enable signal and background to be distinguished for weak beams, often can be applied directly at REX-ISOLDE or be adapted to the acceleration of radioactive beams. This cross fertilization between methods for production, acceleration and measurements of radioactive beams continues unabated and will be an important factor for the future competitiveness of the facility.

Another important factor for the future of REX-ISOLDE is of course upgrades of the machine. A general major upgrade of ISOLDE, the HIE-ISOLDE project [115, 116], has recently been approved at CERN. Improvements of the accelerated beams indeed constitute a major component of HIE-ISOLDE that also includes increases of the primary proton driver beam intensity and several improvements in the low-energy parts of ISOLDE, some of which
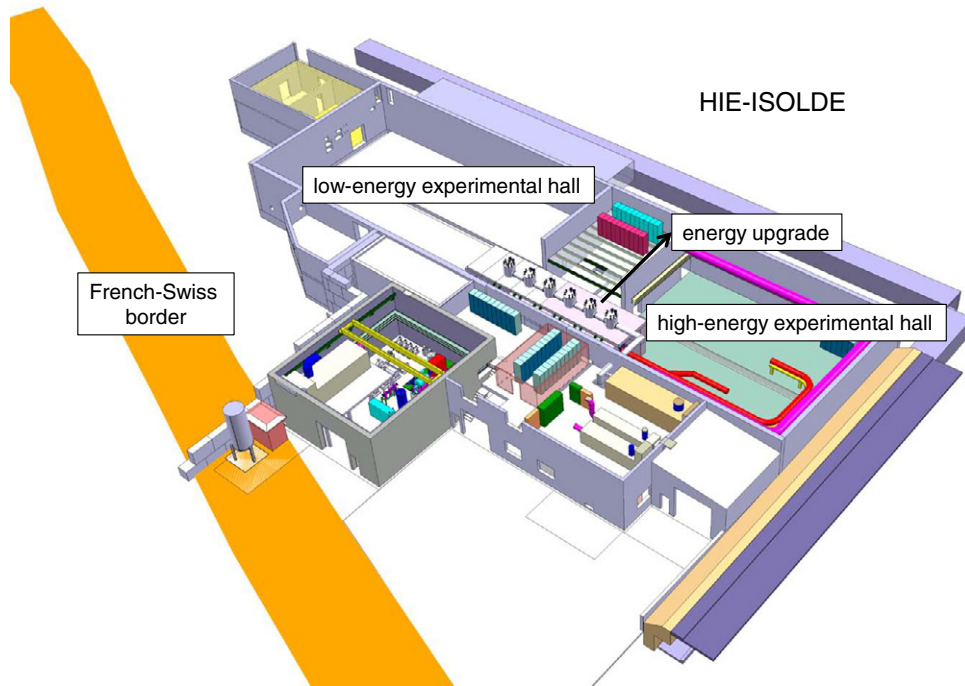
Figure 13. Layout of the HIE-ISOLDE experimental hall and service buildings. The addition of the super conducting cavities will bring the energy of ISOLDE's RIB from the current 3 MeV u^{-1} up to 10 MeV u^{-1}.

will of course also lead to better accelerated beams. The plans are to replace the current linac with a superconducting linac that will be installed in stages (see figure 13). The aim of the first stage is to add cavities that will increase the energy of the beams to 5.5 MeV u^{-1}. This would allow multi-step Coulomb excitation to be performed efficiently for all radioactive beams that can be produced at ISOLDE; furthermore, the conditions for transfer experiments would be improved. A second stage where the energy is raised to 10 MeV u^{-1} would enable more extensive studies involving transfer reactions also using heavy mass beams ($A \sim 200$). Initial physics opportunities are described in [116], while recent updates are posted on the ISOLDE website [117]. The low-energy stage of REX-ISOLDE is also planned to be upgraded so that charge breeding of the radioactive ions can take place faster thereby reducing the delay losses and increasing the efficiency in particular for heavy-mass accelerated radioactive beams.

Acknowledgments

References

[1] Blomqvist J 1967 *Ark. Fys.* **36** 681
[2] Hansen P G 1996 *History of CERN* ed J Krige (Amsterdam: North-Holland) vol 3 p 327

[3]　Haas H, Ravn H, Schempp A, Allardyce B W, Jonson B and Rolfs C 1990 *Proc. 1st Int. Conf. on Radioactive Nuclear Beams (1989 Berkeley)* ed W D Myers *et al* (Singapore: World Scientific) p 59

[4]　Huyse M and Raabe R 2011 *J. Phys. G: Nucl. Part. Phys.* **38** 024001

[5]　Jonson B and Warner D D 1992 *Int. Workshop on the Physics and Techniques of Secondary Nuclear Beams (1992 Dourdan)* ed J F Burandet *et al* (Gif-sur-Yvette: Frontieres) p 355

[6]　Forkel-Wirth D and Bollen G (ed) 2000 *Hyperfine Interact.* **129** 1

[7]　Habs D *et al* 1994 Radioactive beam experiments at ISOLDE: Coulomb excitation and neutron transfer reactions of exotic nuclei *Proposal to the ISOLDE Committee* CERN/ISC 94-25 ISC/P68

[8]　Habs D *et al* 1998 *Nucl. Instrum. Methods* B **139** 128

[9]　Kester O *et al* 2000 *Hyperfine Interact.* **129** 43

[10]　Kester O *et al* 2003 *Nucl. Instrum. Methods* B **204** 20

[11]　Cederkall J *et al* 2004 *Nucl. Phys.* A **746** 17

[12]　Ames F, Cederkall J, Sieber T and Wenander F 2005 The REX ISOLDE Facility: Design and Commissioning Report *CERN Report* CERN-2005-009

[13]　Voulot D, Wenander F, Piselli E, Scrivens R, Lindroos M, Jeppesen H B, Fraile L M, Sturm S and Delahaye P and the REX ISOLDE Collaboration 2008 *Nucl. Instrum. Methods* B **266** 4103

[14]　Habs D *et al* 2000 *Hyperfine Interact.* **129** 43

[15]　Mané E *et al* 2009 *Eur. Phys. J.* A **42** 503

[16]　Kugler E 2000 *Hyperfine Interact.* **129** 23

[17]　Mishin V I, Fedoseyev V N, Kluge H J, Letokhov V S, Ravn H L, Scheerer F, Shirakabe Y, Sundell S, Tengblad O and the ISOLDE Collaboration 1993 *Nucl. Instrum. Methods* B **73** 550

[18]　Köster U *et al* 2003 *Nucl. Instrum. Methods* B **204** 347

[19]　Van Roosbroeck J *et al* 2004 *Phys. Rev. Lett.* **92** 112501

[20]　Lettry J *et al* 1997 *Nucl. Instrum. Methods* B **126** 130

[21]　Bree N *et al* 2008 *Phys. Rev.* C **78** 047301

[22]　Herlert A *et al* 2006 *Int. Symp. on Nuclear Astrophysics* Nuclei in the Cosmos IX *Proc. Sci.* **PoS(NIC IX)051**

[23]　Ames F *et al* 2005 *Nucl. Instrum. Methods* A **538** 17

[24]　Wolf B *et al* 2002 *Rev. Sci. Instrum.* **73** 682

[25]　Sieber T *et al* 2002 *Nucl. Phys.* A **701** 656

[26]　Van de Walle E *et al* 2007 *Phys. Rev. Lett.* **99** 142501

[27]　Van de Walle E *et al* 2009 *Phys. Rev.* C **79** 014309

[28]　Catherall R *et al* 2003 *Nucl. Instrum. Methods* B **204** 235

[29]　Köster U *et al* 2008 *Nucl. Instrum. Methods* B **266** 4229

[30]　Van de Walle E *et al* 2009 *Eur. Phys. J.* A **42** 401

[31]　Hurst A M *et al* 2007 *Phys. Rev. Lett.* **98** 072501

[32]　Eberth J *et al* 2001 *Prog. Part. Nucl. Phys.* **46** 389

[33]　Ostrowski A *et al* 2002 *Nucl. Instrum. Methods* A **480** 448

[34]　Jeppesen H B *et al* 2005 *Nucl. Phys.* A **748** 374

[35]　Tengborn E 2009 Transfer reactions in inverse kinematics at REX ISOLDE *PhD Thesis* Chalmers University of Technology

[36]　Acosta L *et al* 2009 *Eur. Phys. J.* A **42** 461

[37]　Tengblad O, Bergmann U C, Fraile L M, Fynbo H O U and Walsh S 2004 *Nucl. Instrum. Methods* A **525** 458

[38]　Bildstein V *et al* 2007 *Prog. Part. Nucl. Phys.* **59** 386

[39]　Kröll Th *et al* 2009 *Proc. Nuclear Structure and Dynamics '09 AIP Conf. Proc.* **1165** 363

[40]　Jonson B 2004 *Phys. Rep.* **389** 1

[41]　Okołowicz J, Płoszajczak M and Rotter I 2003 *Phys. Rep.* **374** 271

[42]　Jensen A S, Riisager K, Fedorov D V and Garrido E 2004 *Rev. Mod. Phys.* **76** 215

[43]　von Oertzen W, Freer M and Kanada En'yo Y 2006 *Phys. Rep.* **432** 43

[44]　Sorlin O and Porquet M-G 2008 *Prog. Part. Nucl. Phys.* **61** 602

[45]　Jeppesen H B *et al* 2006 *Phys. Lett.* B **635** 17

[46]　Jeppesen H B *et al* 2006 *Phys. Lett.* B **642** 449

[47]　Audi G, Wapstra A H and Thibault C 2003 *Nucl. Phys.* A **729** 337

[48]　Tilley D R, Kelley J H, Godwin J L, Millener D J, Purcell J E, Sheu C G and Weller H R 2004 *Nucl. Phys.* A **745** 155

[49]　Kirsebom O *et al* 2010 in preparation

[50]　Raabe R *et al* 2008 *Phys. Rev. Lett.* **101** 212501

[51]　Kanungo R *et al* 2008 *Phys. Lett.* B **660** 26

[52]　Guo B *et al* 2005 *Nucl. Phys.* A **761** 162

[53] Gade A *et al* 2008 *Phys. Rev.* C **77** 044306
[54] Lee J *et al* 2010 *Phys. Rev. Lett.* **104** 112701
[55] Lee J, Tostevin J A, Brown B A, Delaunay F, Lynch W G, Saelim M J and Tsang M B 2006 *Phys. Rev.* C **73** 044608
[56] Timofeyuk N K 2009 *Phys. Rev. Lett.* **103** 242501
[57] Geithner W *et al* 1999 *Phys. Rev. Lett* **83** 3792
[58] Fortier S *et al* 1999 *Phys. Lett.* B **461** 22
[59] Kanungo R *et al* 2010 *Phys. Lett.* B **682** 391
[60] Keeley N, Raabe R, Alamanos N and Sida J L 2007 *Prog. Part. Nucl. Phys.* **59** 579
[61] Di Pietro A *et al* 2010 *Phys. Rev. Lett.* **105** 022701
[62] Honma M *et al* 2009 *Phys. Rev.* C **80** 064323
[63] Sieja K *et al* 2009 *Phys. Rev.* C **79** 064310
[64] Otsuka T *et al* 2010 *Phys. Rev. Lett.* **104** 012501
[65] Smirnova N A *et al* 2010 *Phys. Lett.* B **686** 109
[66] Yordanov D T *et al* 2007 *Phys. Rev. Lett.* **99** 212501
[67] Gade A *et al* 2007 *Phys. Rev. Lett.* **99** 072502
[68] Motobayashi T *et al* 1995 *Phys. Lett.* B **346** 9
[69] Terry J R *et al* 2008 *Phys. Rev.* C **77** 014316
[70] Caurier E *et al* 1998 *Phys. Rev.* C **58** 2033
[71] Otsuka T *et al* 2001 *Phys. Rev. Lett.* **87** 082502
[72] Niedermaier O *et al* 2005 *Phys. Rev. Lett.* **94** 172501
[73] Scheit H *et al* 2010 to be published
[74] Scheit H *et al* 2004 *Nucl. Phys.* A **746** 96c
[75] Niedermaier O *et al* 2005 *PhD Thesis* University of Heidelberg (www.ub.uni-heidelberg.de/archiv/5647/)
[76] Wimmer K *et al* 2010 *Phys. Rev. Lett.* **105** 252501
[77] Blank B 2009 *The Euroschool Lectures on Physics with Exotic Beams* vol 3 *(Lecture Notes Physics* vol 764*)* (Berlin: Springer) p 153
[78] Lisetskiy A F *et al* 2003 *Phys. Rev.* C **68** 034316
[79] Honma M *et al* 2004 *Phys. Rev.* C **69** 034335
[80] Hosmer P T *et al* 2005 *Phys. Rev. Lett.* **94** 112501
[81] Van Roosbroeck J *et al* 2004 *Phys. Rev. Lett.* **92** 112501
[82] Pauwels D *et al* 2008 *Phys. Rev.* C **78** 041307
[83] Ferrer R *et al* 2010 *Phys. Rev.* C **81** 044318
[84] Stefanescu I *et al* 2007 *Phys. Rev. Lett.* **98** 122701
[85] Stefanescu I *et al* 2008 *Phys. Rev. Lett.* **100** 112502
[86] Sorlin O *et al* 2002 *Phys. Rev. Lett.* **88** 092501
[87] Franchoo S *et al* 1998 *Phys. Rev. Lett.* **81** 3100
[88] Daugas J M *et al* 2010 *Phys. Rev.* C **81** 034304
[89] Flanagan K T *et al* 2009 *Phys. Rev. Lett.* **103** 142501
[90] Banu A *et al* 2005 *Phys. Rev.* C **72** 061305
[91] Ekström A *et al* 2008 *Phys. Rev. Lett.* **101** 012502
[92] Cederkall J *et al* 2007 *Phys. Rev. Lett.* **98** 172501
[93] Ekström A *et al* 2009 *Phys. Rev.* C **80** 054302
[94] Kröll T *et al* 2008 *Int. Conf. on Frontiers in Nuclear Structure, Astrophysics and Reactions (FINUSTAR) CP1012, AIP Conf. Proc.* **1012** 84
[95] Beene J R, Bardayan D W, Galindo Uribarri A, Gross C J, Jones K L, Liang J F, Nazarewicz W, Stracener D W, Tatum B A and Varner R L 2011 *J. Phys. G: Nucl. Part. Phys.* **38** 024002
[96] Radford D *et al* 2002 *Phys. Rev. Lett.* **88** 222501
[97] Grodzins L *et al* 1962 *Phys. Lett.* B **2** 88
[98] Görgen A *et al* 2010 *J. Phys. G: Nucl. Part. Phys.* **37** 103101
[99] Sabbey B *et al* 2007 *Phys. Rev.* C **75** 044305
[100] Hellemans V *et al* 2005 *Phys. Rev.* C **71** 034308
[101] Ljungvall J *et al* 2008 *Phys. Rev. Lett.* **100** 102502
[102] Bonn J *et al* 1972 *Phys. Lett.* B **38** 308
[103] Andreyev A N *et al* 2000 *Nature* **405** 430
[104] Petts A *et al* 2009 *Capture Gamma-Ray Spectroscopy and Related Topics CP1090, AIP Conf. Proc.* **1090** 414
[105] Grahn A *et al* 2009 *Phys. Rev.* C **80** 014324
[106] Jungclaus A *et al* 2008 *Proposal to the ISOLDE Committee* CERN/INTC IS483

[107] Lindroos M *et al* 2000 *Hyperfine Interact.* **129** 109
[108] Jenkins D G, Glover R, Herzberg R D, Boston A J, Gray-Jones C and Nordlund A 2009 *Nucl. Instrum. Methods* A **602** 457
[109] Ball G C, Buchmann L, Davids B, Kanungo R, Ruiz C and Svensson C E 2011 *J. Phys. G: Nucl. Part. Phys.* **38** 024003
[110] Grawe H, Langanke K and Martínez-Pinedo G 2007 *Rep. Prog. Phys.* **70** 1525
[111] Langanke K, Thielemann F-K and Wiescher M (ed) 2006 Special issue on nuclear astrophysics *Nucl. Phys.* A **777** 1
[112] Woods P J 2009 *Nucl. Phys.* A **827** 582c
[113] José J and Hernanz M 2007 *J. Phys. G: Nucl. Part. Phys.* **34** R431
[114] He J J *et al* 2009 *Phys. Rev.* C **80** 042801
[115] Lindroos M and Nilsson T (ed) 2006 HIE ISOLDE: the technical options *CERN report* CERN-2006-013
[116] Riisager K, Butler P, Huyse M and Krücken R (ed) 2007 HIE ISOLDE: the scientific opportunities *CERN report* CERN-2007-008
[117] ISOLDE website 2010 http://isolde.web.cern.ch/ISOLDE/